© Indian Academy of Sciences

Investigation of 2T Pb-free wide bandgap perovskite/c-Si tandem device through simulation by SCAPS-1D

SHIVANI CHAUHAN* and RACHNA SINGH

Department of Electronics and Communication, Jaypee Institute of Information Technology, Noida 201309, India
e-mail: 20402002@mail.jiit.ac.in; rachna.singh@mail.jiit.ac.in

Abstract.   Shockley Queisser's theory states that the efficiency of single-junction solar cells is restricted. This constraint can be avoided by employing a tandem (stacking multiple cells) setup. Furthermore, stacking layers such as Perovskite/silicon in tandem architecture might boost efficiency. In this research, SCAPD-1D was used to simulate a monolithic 2T Perovskite/silicon tandem solar cell. The tandem configuration is composed of a narrow bandgap (1.1 eV) crystalline silicon Heterojunction with an intrinsic thin layer (HIT) solar cell at the bottom and a wide bandgap (1.8 eV) lead-free Perovskite ($Cs_2AgBi_{0.75}Sb_{0.25}Br_6$) solar cell on top. The proposed tandem device is simulated as a standalone and integrated structure. The PCE of the calibrated standalone cell is 14.54% (top cell) and 21.66% (bottom cell), respectively. The calibrated cells are used to design an integrated tandem configuration. The current matching condition is accomplished at varied thicknesses of top and bottom absorber layers. A bottom cell's ideal current matching thickness is 230 μm, while a perovskite top cell is 550 nm. The overall conversion efficiency of the tandem device is 26%, with an FF of 79.18%.

Keywords.   Perovskite; tandem solar cell; monolithic.

1. Introduction

Solar photovoltaic (PV) energy is a renewable energy source that is both abundant and clean. In 1839, the photovoltaic was first introduced by Henri Becquerel [1], but the first p-n junction solar cell was invented in 1940 at Bell's lab by Russell Shoemaker Ohl [2]. Further, the Bell lab announced the first silicon-based single junction solar cell in 1954 [3]. In 1961, for single-junction solar cells, William Shockley and Hans-Joachim Queisser determined the theoretical limit, termed the S-Q limit, to be 33% [4]. This limits the maximum output of the single-junction solar cell. The solar spectrum should be better utilized to move ahead of this S-Q limit. This is achieved by stacking or combining multiple cells with different bandgaps, each of which absorbs photons in another band. When two absorbing layers of different bandgap are stacked, this representation is called tandem. The Architecture of tandem device is implemented as mechanically stacked, monolithically integrated and spectral split. Tandem modules are categorized as 2T, 3T, and 4T depending on whether cells are coupled in series or parallel [5]. The tandem device is also capable of reducing electrical (thermalization loss) and optical losses (transmission loss). The silicon and perovskite make a powerful combination for a tandem device, as the perovskite layer effectively uses the solar energy in the visible spectrum whereas the silicon converts the IR (Infrared) components into electrical energy [6]. The mineral Perovskite is named after the prominent Russian mineralogist Perovski [7]. The perovskite molecular formula is ABX_3, where A and B are different sizes of cations and X is a halide (Br, I, F) [8]. Also, perovskite shows amazing properties i.e., less exciton binding energy, high absorption coefficient ($>0.5 \times 10^4$ cm^{-1}), tunable bandgap (1.1–2.3 eV), mobility of electron (~ 5–10 cm^2 V^{-1} s^{-1}), mobility of hole (~ 1–5 cm^2 V^{-1} s^{-1}), [9] long diffusion length (~ 175 μm), fast charge separation and low processing cost which makes it an ideal material for wide band gap [10]. The first 2T PVSK/Si was presented in 2015 at PCE 13.7% [11]. The PCE of this cell is limited by the lower photocurrent. In recent records, the perovskite standalone PCE reaches 25.6% [12]. This improved performance of perovskite leads to the PVSK/Si tandem solar cell. Recently the PCE for 2T PVSK/Si tandem has reached 29.15% [13]. Because a single transparent conductive electrode is required for a 2T tandem device, parasitic loss and fabrication costs are reduced. Extensive research has been undertaken in recent years with an emphasis on perovskite absorber thickness, defect densities, interface defect

*For correspondence

densities, recombination layer investigations, and bottom silicon cell structure. The conversion efficiency is influenced by physical properties such as defect density, temperature and thickness. Several studies have revealed how the defect density [14–18] and the thickness of the absorber layer affect the device's PV characteristics [19, 20]. The performance of the device is reduced by increasing the defect density. Frankel and Schottky defect highly affect the Voc and diffusion length of PVSK-based solar cells. HTL/perovskite interface defects affect the Voc, while PVSK/ETL interface defects impact Jsc [21]. Literature [22] reveals that a higher recombination rate reduces the lifetime and diffusion length of carriers of the PVSK absorber layer by increasing the defect density.

The high PCE and high Voc of SHJ solar cells, which typically exceed 730 mV, make them promising for use as bottom cells in tandem combinations. To explore the potential of PVSK/Si proper optimization of absorber thickness and current matching need to be brought off. According to [23] Qiu *et al*, raising the bandgap improves the PCE of tandem devices by increasing the Voc and decreasing the Jsc. This study aims to use SCAPS-1D to model a PVSK-based solar device that is entirely free of lead. A monolithic 2T PVSK/Si tandem solar cell simulation model has been improved. To improve the performance of the tandem structure, a reported top and bottom structure are chosen [24, 25]. By optimizing the layer thicknesses for both cells current matching condition was determined. PV parameters like as Voc, Jsc, FF, and PCE could be optimized via simulation. Our optimized tandem cell delivers 26% efficiency with 18.1 mA cm^{-2} Jsc in each sub cell.

2. Simulation methodology and device simulation

2.1 *Methodology*

The device is modeled using SCAPS-1D (Solar Cell Capacitance Simulator) software version 3.3.09. It is a 1D solar cell simulator developed by the Electronics and Information Systems (ELIS) department at the University of Gent [26]. This software simulates almost all parameters of solar cell up to seven semiconductor layers. The user can set the operating points such as voltage, frequency, thickness, illumination and temperature and depict the result in the form of different PV parameters, EQE curve, J-V curve, Energy band diagrams, generation and recombination profiles [27, 28]. SCAPS 1D is a programme that solves the fundamental equations. A polished planar heterojunction structure is considered for simulation in this paper, and several obstacles are investigated in [29] for textured silicon on perovskites. It is difficult to choose an analysis tool due to the difference in thickness between textured silicon and perovskite layers. 2-D effects could be simulated by TCAD and COMSOL, as well as other simulators. For modelling of electrical properties, the Poisson's equation

for electrons and holes (1), the electron continuity equation (2), the hole continuity equation (3), and the carrier transport equations for electrons (4) and holes (5) are utilized [30].

$$\frac{\partial}{\partial x}\left(\varepsilon_0\varepsilon\frac{\partial\psi}{\partial x}\right) = -q(p - n + N_D^+ - N_A^- + p_t - n_t) \quad (1)$$

$$\frac{-\partial J_n}{\partial x} - U_n + G = \frac{\partial n}{\partial t} \quad (2)$$

$$-\frac{\partial J_p}{\partial x} - U_p + G = \frac{\partial p}{\partial t} \quad (3)$$

$$J_n = D_n\frac{\mathrm{d}n}{\mathrm{d}x} + \mu_n n\frac{\mathrm{d}\phi}{\mathrm{d}x} \quad (4)$$

$$J_p = D_p\frac{\mathrm{d}p}{\mathrm{d}x} + \mu_n p\frac{\mathrm{d}\phi}{\mathrm{d}x} \quad (5)$$

SCAPS-1D's distinguishing qualities include the ability to model the cell structure with defects such as interface and charge type (no charge, monovalent, divalent or amphoteric) [28]. It has been shown in Olyaeefar *et at* [31] that surface recombination velocities can be determined by defect densities. The study by Siekmann *et al* [32] explores the simulation of SCAPS using drift-diffusion and other defects. The equation of efficiency η (%) if given by

$$\eta = \frac{Jsc \times Voc \times FF}{Pin} \quad (6)$$

$$\text{Voc} = \frac{nkT}{q}\ln\left(\frac{I_l}{I_0} + 1\right) \quad (7)$$

From equation (7), Voc depends on light generated current and the saturation current. Io also depends on the recombination, as the recombination current reduce, the Voc increases with the bandgap. The thickness tells how much light is absorbed by the absorber layer. For top cell thickness, a plot of the AM1.5G spectrum and the filtered spectrum used to generate the bottom cell in tandem is shown in figure 1. The abbreviations are given in table 1.

2.2 *Device structure*

SCAPS-1D does not support the multi-junction simulation. Before integrating the top and bottom cell into monolithic tandem both sub cell is independently optimized. First the top cell is illuminated with AM1.5G solar spectrum has an integrated power of 1000 W/m^2 [33]. The top module is composed of a lead-free 1.8 eV wide bandgap (Cs$_2$AgBi$_{0.75}$Sb$_{0.25}$Br$_6$) PVSK absorber layer whose thickness is varied from 50 to 700 nm, 40 nm phenyl-C61-butyric acid methyl ester (PCBM)/10 nm Tin Oxide (SnO$_2$) as ETL, 40 nm Copper thiocyanate (CuSCN) as HTL respectively as shown in figure 1. Equation (8) represents the top cell's transmitted spectrum at various absorber thicknesses.
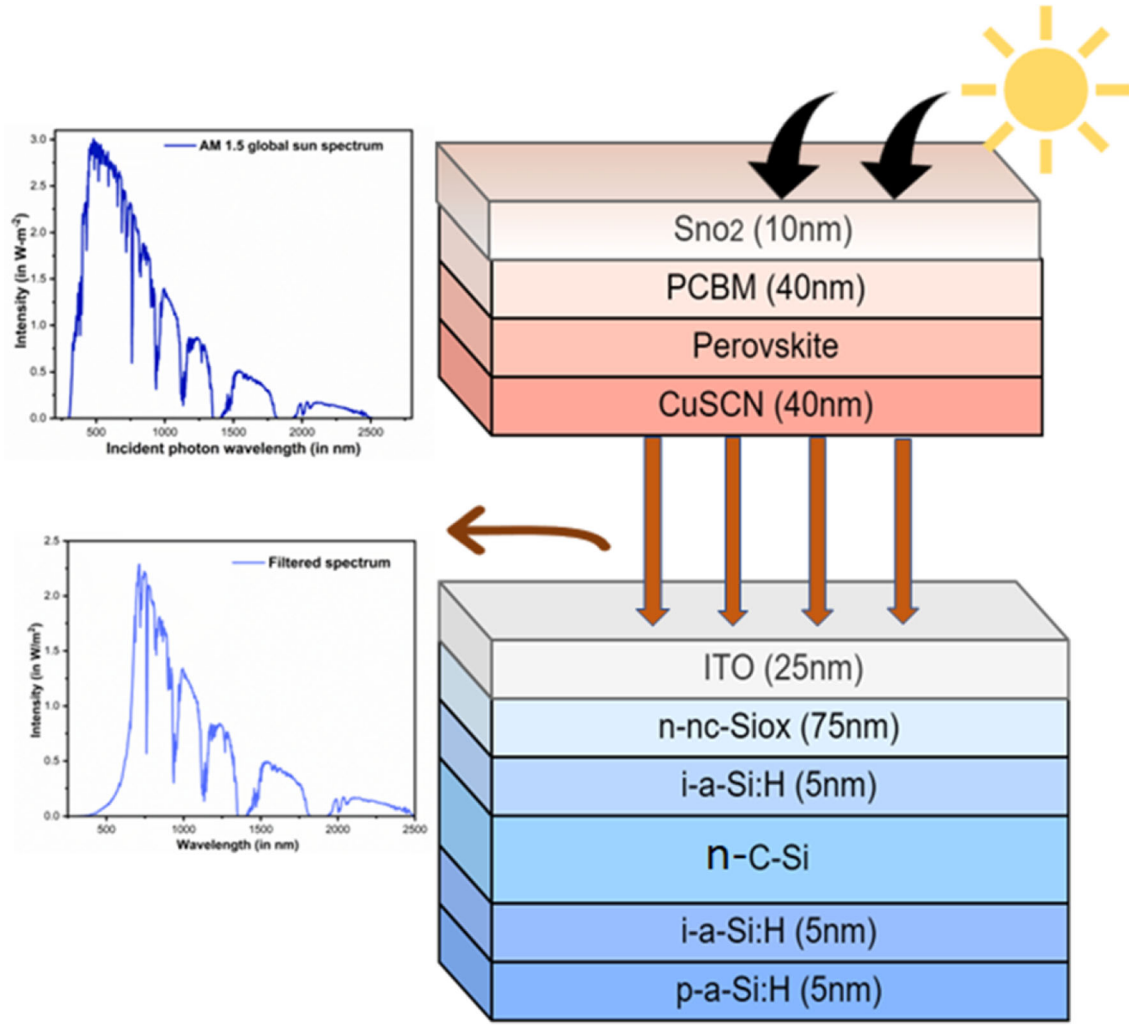
Figure 1. Tandem cell schematic, with top cell at AM1.5 spectrum and bottom cell at filtered spectrum.

$$S(\lambda) = s_0(\lambda).exp(\sum_{i=1}^{4} -(a_{material_i}(\lambda).d_{material_i})) \quad (8)$$

S0(λ) is incident AM1.5 spectrum, the layer thickness is d, and the absorption coefficient is α. The interfacial reflection losses are not taken into account. $material_i$ (i = 1, 2, 3, 4) corresponds to CuSCN, WBH PVSK, Sno$_2$, PCBM, respectively. A n-type C-Si wafer with an ideal thickness of 250 m and a layer stack of 5 nm i-a-Si:H, 75 nm n-nc-SiOx, and 25 nm ITO compensate the SHJ cell. On the rear side, an intrinsic (i-a-Si:H) layer of 5 nm and p-doped a-Si:H layer of thickness 5 nm are stack respectively as shown in figure 1. An exhaustive literature search is conducted to gather the electrical and optical parameters, as well as the interface defect densities of the materials employed in the simulation, which are presented in supporting information S1. Considering the N_t defect density in PVSK layer of 2.5×10^{13} cm^{-3} with gaussian distribution

and a characterization energy of 0.1 eV and carrier lifetime of 200 ns determined by

$$\tau_n = \frac{1}{\sigma_n v_{th} N_t}, \tau_p = \frac{1}{\sigma_p v_{th} N_t} \quad (9)$$

Here σ_n and σ_p is the cross-section area of holes and electrons which is 2×10^{-14} cm^2 for PVSK layer, v_{th} is the thermal velocity which is (10^7 cm/s). In addition, the L_D (carrier diffusion length) for holes and electron is 1 μm determined by

$$L_D = \sqrt{D\tau} \quad (10)$$

$$D = \frac{\mu K_B T}{q} \quad (11)$$

It is believed that the good optoelectronic capabilities of hybrid lead halide perovskite are attributable to the

Table 1. Throughout the paper, common notation and abbreviations are used.

ε_0 = permittivity of free space	AM 1.5 = Air mass 1.5 spectra	R_{Sh} = shunt resistance
Dp/Dn = Diffusion Coefficient of holes and electron	η = PCE or Power Conversion Efficiency	J_p/J_n = current density due to holes/electron
ε = permittivity of material	p_t = trapped hole	Eg = band gap
n_t = trapped electron	Nc = Density of states in conduction band	e = electronic charge
N_V = Density of state in valence band	n = electron concentration	p = hole concentration
χ = electron affinity	Un = electron recombination rate	N_A^+/N_D^- = ionized acceptor/donor density
N_D/N_A = Donor and acceptor density	R_S = series resistance	HTL = hole transport layer
ETL = Electron Transport layer	$\mu p/\mu n$ = hole/electron mobility	V_{OC} = open-circuit voltage
G = hole/electron generation rate	Ec = conduction band minimum	CB = conduction band
J_{SC} = short-circuit current density	EQE = external quantum efficiency	PVSK = Perovskite
FF = fill factor	SHJ = Silicon Heterojunction	WBH = Wide band Halide
FC = front contact	Pin = Incident power	BC = back contact
V_{max} = maximum power point Voltage	J_{max} = maximum power point current	Io = Dark saturation current
VB = Valence band	σn (cm^2) = electron capture cross-section	σp (cm^2) = hole capture cross-section

electronic arrangement of Pb, therefore replacing Pb with Sb would be ideal [34]. Experiment findings are used to calculate the absorption coefficient for all materials [9, 35–37]. Both the top and bottom cells are calibrated according to the results of the work reported in [38] to have a 10.08% efficient top cell and a 20.5% efficient bottom cell, respectively [39].

In order to accomplish the tandem device, the filtered spectrum is used to simulate the bottom cell for current matching conditions. The findings and discussion section contains a full explanation of the current matching and filter spectrum approach. The interfacial defects at heterojunction are considered and reported in supporting information Table S2. Furthermore, amphoteric defects for intrinsic and p-type i-a-Si:H are addressed in S3. During simulation, the semiconductor equations and the basic equations for SCAPS' optical model are used.

3. Result and discussion

There are three sub-sections in this section. The device is first simulated in a stand-alone mode. Sections 3.1 and 3.2 contain detailed calibration and simulation information. The device is then assembled to produce a 2T monolithic tandem device, as shown in section 3.3.

3.1 *Top and bottom cell optimization in a stand-alone situation*

For the optimum function of tandem device high bandgap of 1.8 eV top absorber layer is chosen. Initially, the top and bottom is calibrated in standalone condition under AM 1.5G solar spectrum. To model PVSK single-junction top cells in the n–i–p "inverted" configuration, we employed

PCBM/SnO2 as the ETL stacked on PVSK absorber layer and CuSCN as the HTL. CuSCN as HTL is a good alternative to Spiro-OMeTAD because of cost effective and stability [40]. A mixed-cation mixed-halide PVSK absorber was employed ($Cs_2AgBi_{0.75}Sb_{0.25}Br_6$) that was devoid of lead. On illumination, the absorber layer generates the electron diffuse to CB of ETL layer and holes are injected into the VB of HTL layer. Then after these carriers are collected by front contact and back contact. The top cell is calibrated at the thickness of 500 nm absorber layer, get 14.54% PCE. The J-V and EQE curves for varied thicknesses of PVSK absorber layer are shown in figure 2. The thickness was varied in fifteen equal steps from 50 to 700 nm on a linear scale, while the remaining layer thicknesses were left unchanged. Increasing thickness enhanced the absorption and lower the transmittance loss. Hence increasing thickness resulted in enhanced EQE, from 50 to 500 nm EQE increases 19.04% → 77.80% in figure 2(b). Although increasing thickness improves EQE, it also limits performance since absorption saturation occurs at larger thicknesses. Jsc increased from 5.98 mA cm^{-2} to 19.31 mA-cm^{-2} as the thickness was increased from 50 nm to 700 nm, suggesting that better optical performance predicts an increase in Jsc. The overall PCE is collective outcome of three parameters FF, Jsc, Voc calculated by using Eq (6). The illuminated J-V characteristics are reported in table 2 (figure 3).

The thickness of the C-Si absorber layer in the SHJ bottom cell varies between 80 μm and 300 μm. The EQE and J-V curves are derived by simulating in thirteen equal steps (see figure 4) for various absorber layer thicknesses under the AM 1.5G spectrum. As the wavelength of the C-Si layer increases, less energetic photons are absorbed. At lower wavelengths, however, as the thickness of C-Si layer increases and the collecting probability decreases, EQE declines. Hence increasing thickness from 80 μm →
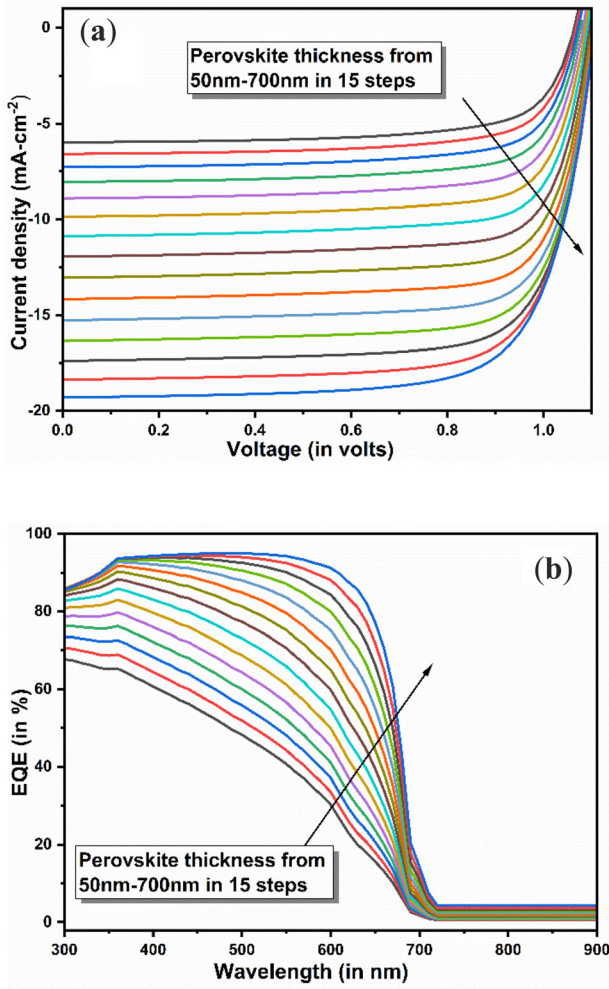
Figure 2. (a) Under AM 1.5G, the J-V curve of the top cell for varied absorber thicknesses (50–700 nm), (b) EQE Curve for top cell at different thickness (50–700 nm) under AM1.5G.
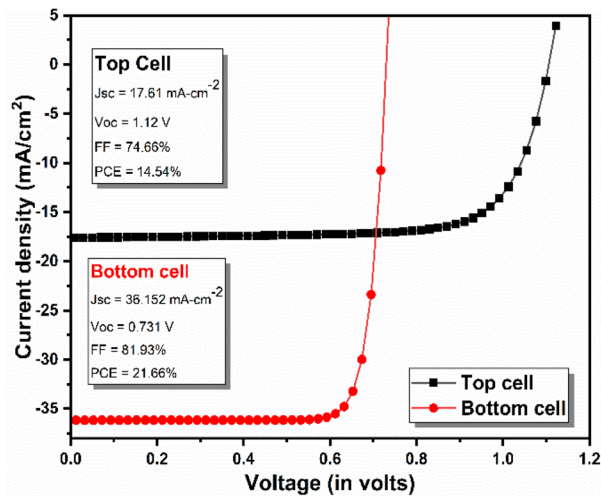

Figure 3. Under the incident AM1.5G spectrum, the J-V curves of the top and bottom cells in standalone mode are shown.
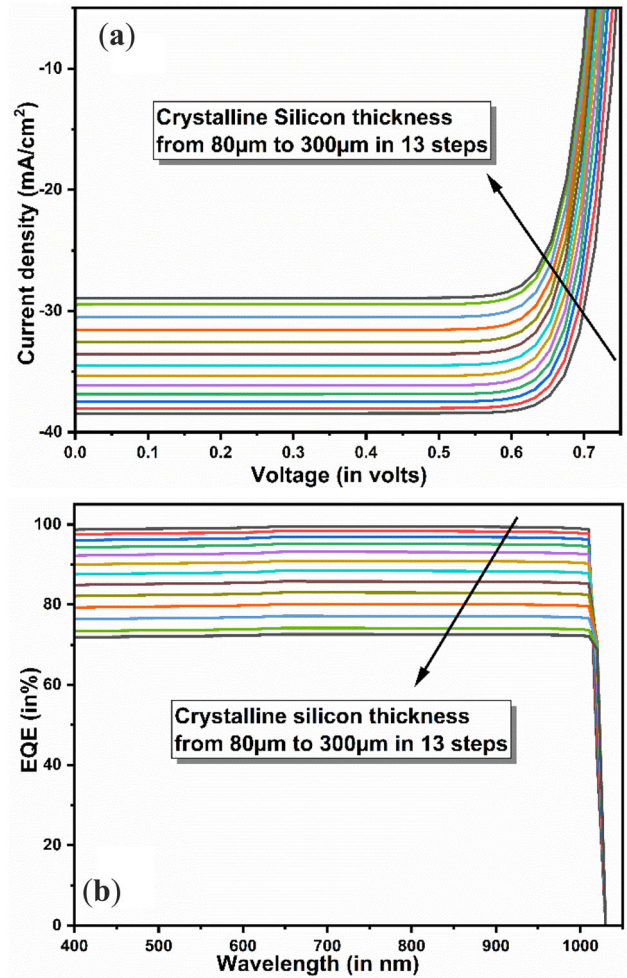

Figure 4. (a) J-V curve and (b) EQE curve at different thickness from 80 μm to 300 μm of bottom C-Si layer under AM1.5G spectrum.

300 μm EQE reduce to 98.88% → 72.5%. The SHJ bottom cell is calibrated at 150 μm. The J-V curve at varied C-Si thicknesses is shown in figure 4(a). The Jsc drops from 38.25 mA cm^{-2} to 28.93 mA cm^{-2} as the thickness increases from 80 μm to 300 μm.

3.2 *The effect of absorber layer thickness on bottom and top cell performance*

The Jsc of the monolithic tandem device's top and bottom cells must be the same. An investigation of the variations in thickness of the top and bottom cells was conducted to obtain the current matching condition. The thickness of the absorber layer influences PV characteristics (Jsc, Voc, FF, PCE). Figure 6 depicts the effect of top cell absorber thickness. To get the optimum value the thickness of PVSK absorber layer varied (80–700 nm) while the other layer's thickness is kept constant.
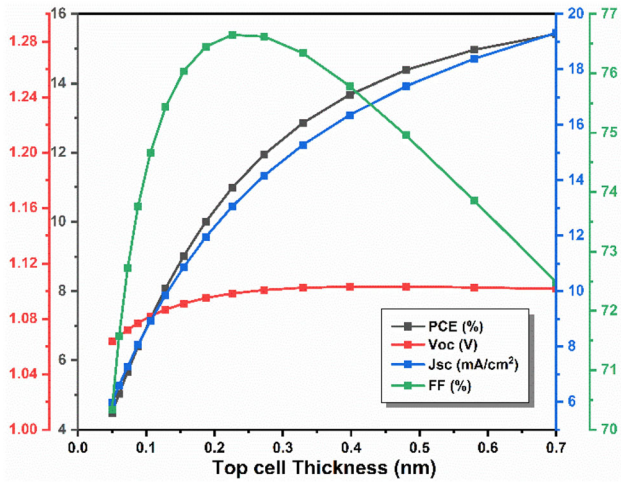
Figure 5. Impact of PVSK absorber thickness (50–700 nm) on PV parameters in standalone configuration.

Figure 6. Impact of thickness of bottom C-Si absorber layer on PV parameters.

Figure 5 plots the results of Voc, Jsc, PCE and FF of top structure with respect to change in PVSK thickness. Value of Jsc and Voc increased from 5.98 mA cm^{-2} to 19.31 mA cm^{-2} and from 1.064 V to 1.12 V with the increase in thickness from 80 nm to 700 nm. Jsc increases with absorber layer thickness due to greater photon absorption in the absorber layer, which leads to an increase in charge carrier production. When the PVSK layer thickens, Jsc and EQE become saturated. The FF reduce as the absorber layer thickness increases. With an increase in thickness from 50 nm to 230 nm, FF increased from 70.34% to 76.6%. Afterwards Increase in thickness own increase in series resistance hence FF reduces at higher thickness of absorber layer. The device FF is defined as follows:

$$FF = \frac{Vmax.Jmax}{Voc.Jsc} \qquad (9)$$

The internal power depletion is concluded by FF, which is a significant metric. Internal power increases while FF drops as the absorber layer thickness increases. The top and bottom cells both show the same pattern. Low energy photons (longer wavelength), which have a greater absorption depth, are absorbed throughout the cell, whereas high energy photons (shorter wavelength) are absorbed close to the surface and have a shorter absorption depth. To absorb the radiation, a thick silicon wafer is required due to silicon's low absorption coefficient. In SHJ bottom cell due to increase in thickness from 80 μm to 300 μm enhance the recombination rate, hence reduce the probability of collecting the generating carriers which results in decrease in Jsc shown in figure 6. The carrier concentration in C-Si(n) is ($\sim 10^{16}$ cm^{-3}) and a-Si:H (p) is ($\sim 10^{20}$ cm^{-3}), several orders higher than absorber layer, hence low built-in potential. Figure 6 depicts the effect of C-Si thickness on PV characteristics. The Voc decreases slightly as the C-Si
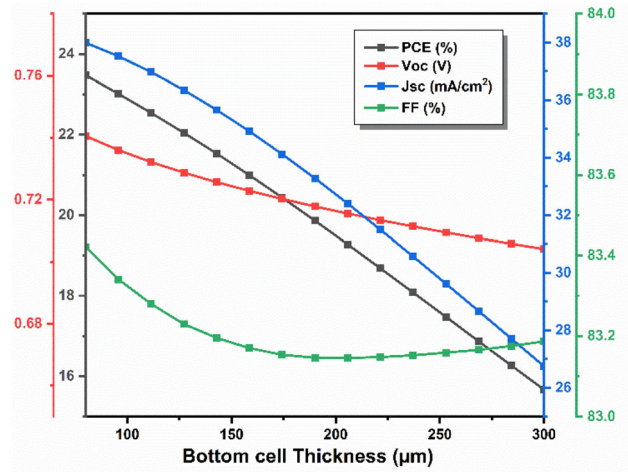
thickness increases due to the electric field strength. The overall PCE of the bottom cell reduced from 23.47% to 15.66% as the thickness of the C-Si increases from 80 μm to 300 μm. The entire device cost is decreased by lowering the C-Si thickness. All PV parameters are summarized in table 2 at thickness of 150 μm which results in PCE of 21.66%. Voc for top cell is higher than Voc for bottom cell because to the large bandgap of Cs$_2$AgBi$_{0.75}$Sb$_{0.25}$Br$_6$ (1.8 eV) whereas top cell Jsc (17.61 mA cm^{-2}) is lower than bottom cell Jsc (36.152 mA cm^{-2}).

3.3 *Monolithic PVSK/Si tandem device*

Top and bottom cells make into a tandem cell. Sub cells with lower Jsc can decrease tandem architecture's overall performance. Burdick and Glatfelter devised this approach in 1986, and it requires the same Jsc for both cells [41]. Because the two sub cells are appropriately connected in series, they must have the same Jsc. To obtain the most Jsc out of a tandem device, materials with different bandgaps should be utilized so that each may perform in its region of the power spectrum. The filtered power spectrum for varied PVSK thicknesses ranging from 80 nm to 700 nm is used to establish current matching conditions. Each filter spectrum discovered in the top cell illuminates the bottom cell for

Table 2. Simulated parameters Voc, Jsc, FF, PCE report in this work under standalone condition.

Parameters	Top cell (500 nm)	Bottom cell (150 μm)
Jsc (mA-cm^{-2})	17.61	36.152
Voc (V)	1.12	.731
FF (%)	74.66	81.93
PCE (%)	14.54	21.66
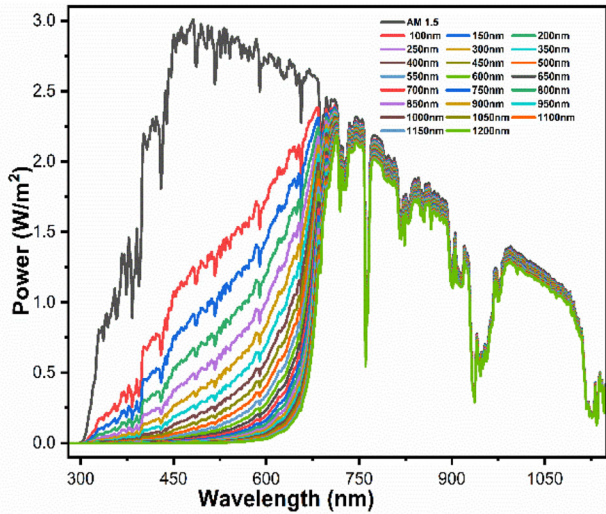
Figure 7. Spectrum emitted by the top cell at various PVK thicknesses ranging from 100 nm to 1200 nm.

Figure 9. PV parameters corresponding to the current matching points.

each thickness of the top absorber layer. Figure 7 shows 23 distinct filter spectrums for various maximum cell thicknesses. For each filter spectrum, the bottom cell is simulated for Jsc by varying the thickness of bottom cell from 50 μm to 300 μm plotted in figure 8. Jsc values of the top cell were plotted against the variable thickness of the top cell in the same graph, demonstrating the current matching condition. The best intersection sites are presented in figure 9 for PVSK thicknesses ranging from 50 nm to 700 nm and C-Si thicknesses ranging from 80 μm to 300 μm. The ideal current matching point among them is chosen to offer the highest tandem Jsc of 18.106 mA-cm^{-2} with 550 nm and 230 μm top and bottom subcell thicknesses, respectively.
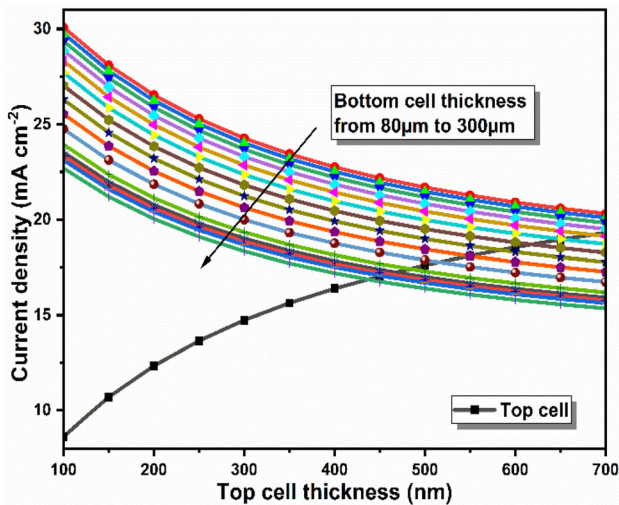

Figure 8. At different thickness (50–700 nm) of the top absorber layer, this curve was utilized to obtain current matching conditions for both the top and bottom cells.
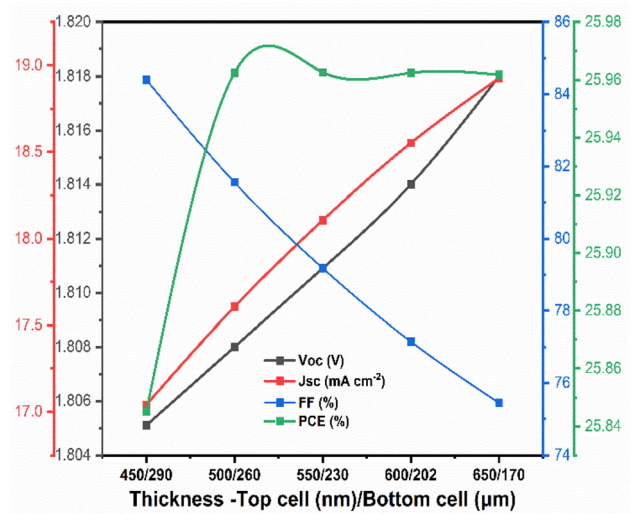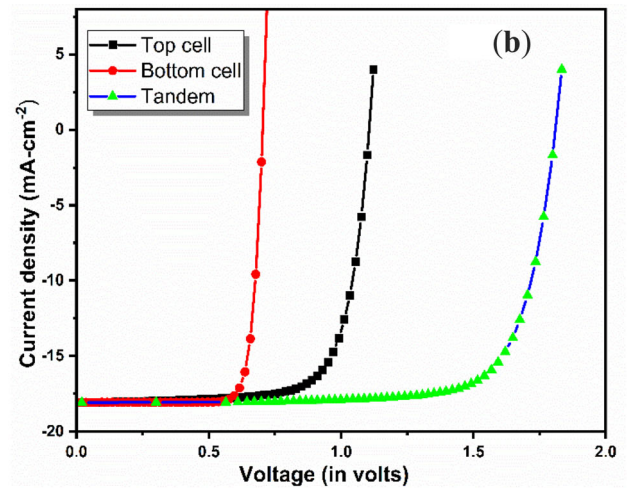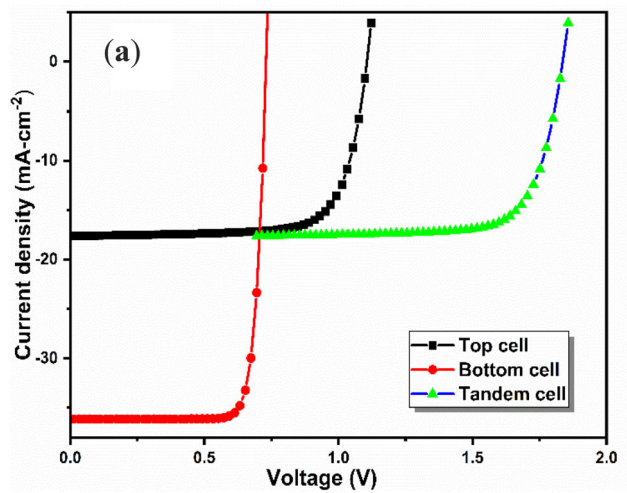

Figure 10. (a) J-V curve shows the limiting top cell under AM1.5G spectrum at optimized thickness. (b) J-V curve for top (under AM1.5G), bottom cell (under with filter spectrum) and tandem cell.

Table 3. Summary of the PV parameters of this device that have been considered.

Parameters	Top cell at 550 nm	Bottom cell under filter spectrum by top cell	Tandem
Jsc (mA-cm^{-2})	18.1068	18.085	18.1068
Voc (V)	1.12	.7044	1.812
FF (%)	74.15	82.97	79.18
PCE (%)	14.85	18.55	25.95

For tandem, the top cell is re-simulated following the Jsc determination under AM1.5G spectrum with a thickness of 550 nm to create a filter spectrum, which is then utilized to illuminate the bottom cell with thickness of 230 μm and acquire the J-V curve under tandem configuration. Figure 10(b) shows the J-V curves for the top cell at 550 nm under AM1.5G and bottom cell at 230 μm under filter spectrum. To make the tandem curve illustrated in figure 10(a), the voltages of both cells at equal current points are added. In terms of Voc, the J-V curve presented in figure 10(b) performs better than the standalone condition. Table 3 presents all PV parameters derived from device structure simulation and analysis.

As both sub cells are coupled in series, the total output voltage is calculated by summing the voltages of both sub cells during current matching conditions. Figure 10(a) shows the J-V curve for tandem, as well as the J-V curves for the top and bottom cells. The top cell, which has a high Voc because of its wide bandgap (1.8 eV) perovskite, is clearly the limiting cell. In terms of Voc, the output performance of the J-V tandem is comparatively better than that of standalone versions. The FF of a tandem device was computed by finding the device's Jmax and Vmax using the maximum power point factor. The J-V curve of the tandem cell and the power curve of the device are shown in figure S1. The FF and Voc of the tandem are 79.18% and 1.812%, respectively. The overall PCE of a PVSK/Si tandem solar cell is 25.95%.

4. Conclusion

In terms of performance and reliability, PVSK/Si tandem solar cells are still in the early stages of research. The performance of SnO$_2$/PCBM/ Cs$_2$AgBi$_{0.75}$Sb$_{0.25}$Br$_6$/ CuSCN and ITO/n-nc-SiOx/i-a-Si:H/n-C-Si/i-a-Si:H/p-a-Si:H solar cells are simulated by using SCAPS-1D. In this work, a lead-free wide bandgap (1.8 eV) PVSK (Cs$_2$-AgBi$_{0.75}$Sb$_{0.25}$Br$_6$) was simulated. Because their bandgaps differ, the two sub cells will feed on different sections of the solar spectrum. The top cell and bottom cells had 14.54% and 21.66% efficiency, respectively, in a stand-alone state. By adjusting the thicknesses of the absorber layer to produce 2-T tandem, the current matching condition was explored. The current matched device at the Jsc = 18.106 mA cm^{-2} at optimized top and bottom cell thickness of 500 nm and 230 μm. The device is further enhanced in tandem arrangement for improved performance. The PV parameters of our tandem structure are: Jsc = 18.106 mA cm^{-2}, Voc = 1.812 V, FF = 79.18% and PCE = 15.98%. The described PVSK/Si provides a way for further advancement in the field of energy conversion system that is lead-free, low cost, and high efficiency.

References

[1] Taguchi M, Suzuki A, Ueoka N and Oku T 2019 Effects of poly(methyl methacrylate) addition to perovskite photovoltaic devices. *AIP Conf. Proc.*, vol. 2067

[2] Szabó L 2017 The history of using solar energy. *Proc. - 2017 Int. Conf. Mod. Power Syst. MPS 2017*, no. June 2017

[3] Fraas LM 2014 Low-cost solar electric power. *Low-Cost Sol. Electr. Power*, **9783319075**(June 2014) 1–181

[4] Monteiro Albuquerque G 2018 Theoretical limit for efficiency of silicon solar cells. *J. Appl. Phys.*

[5] Jimeno J C, Gutierrez R and Fano V 2016 A 3 Terminal Parallel Connected Silicon Tandem Solar Cell. *Energy Procedia* 92: 644–651

[6] Akhil S, Akash S and Pasha A 2021 Review on perovskite silicon tandem solar cells: Status and prospects 2T, 3T and 4T for real world conditions. *Mater. Des.* 211: 110138

[7] Rhodes C J 2014 Perovskites and their potential use in solar energy applications. *Sci. Prog.* 97(3): 279–287

[8] Ansari M I H, Qurashi A and Nazeeruddin M K 2018 Frontiers, opportunities, and challenges in perovskite solar cells: A critical review. *J. Photochem. Photobiol. C Photochem. Rev.* 35: 1–24

[9] Madan J, Shivani Pandey R and Sharma R 2019 Device simulation of 17.3% efficient lead-free all-perovskite tandem solar cell. *Sol. Energy* 197: 212–221

[10] Jamal M S, Shahahmadi S A and Chelvanathan P 2019 Effect of defect density and energy level mismatch on the performance of perovskite solar cells by numerical simulation. *Optik (Stuttg)* 182: 1204–1210

[11] Mailoa J P, Bailie C D and Johlin E C 2015 A 2-terminal perovskite/silicon multijunction solar cell enabled by a silicon tunnel junction. *Appl. Phys. Lett.* 106(12)

[12] Jeong J, Kim M, Seo J, Lu H, Ahlawat P, Mishra A, Yang Y, Hope M A, Eickemeyer F T, Kim M, Yoon Y J, Choi I W, Choi S J, Lee J H, Kim D S, Kim J Y, Gratzel M and Emsley L 2021 Pseudo-halide anion engineering for α-FAPbI3 perovskite solar cells. *Nature* 592(7854): 381–385

[13] Cheng Y and Ding L 2021 Perovskite/Si tandem solar cells: Fundamentals, advances, challenges, and novel applications. *SusMat* 1(3): 324–344

[14] Decock K, Khelifi S and Burgelman M 2011 Modelling multivalent defects in thin film solar cells. *Thin Solid Films* 519(21): 7481–7484

[15] Dahlal Z, Hamdache F, Rached D and Rahal W L 2021 Deep Impact of the n-c-Si Defect Density on Heterojunction with Intrinsic Thin Layer Solar Cells. *J. Nano- Electron. Phys.* 13(6): 1–4

[16] Astakhov O, Smirnov V, Carius R, Petrusenko Y, Borysenko V and Finger F 2014 Relationship between absorber layer defect density and performance of a-Si: H and μc-Si: H solar cells studied over a wide range of defect densities generated by 2 MeV electron bombardment. *Sol. Energy Mater. Sol. Cells* 129: 17–31

[17] Dubey S, Mathur A S and N and Singh B, 2019 Effect of defect density in different layers and ambient temperature of n-i-p a-Si single junction solar cells performance. *Int. J. Sci. Res. Phys. Appl. Sci.* 7(2): 93–98

[18] Ouslimane T, Et-taya L, Elmaimouni L and Benami A 2021 Impact of absorber layer thickness, defect density, and operating temperature on the performance of MAPbI3 solar cells based on ZnO electron transporting material. *Heliyon* 7(3): e06379

[19] Zekry A, Shaker A and Salem M 2018 *Solar Cells and Arrays: Principles, Analysis, and Design. Advances in Renewable Energies and Power Technologies* **1**

[20] Mandadapu U, Vedanayakam S V, Thyagarajan K, Reddy M R and Babu B J 2017 Design and simulation of high efficiency tin halide perovskite solar cell. *Int. J. Renew. Energy Res.* 7(4): 1604–1612

[21] Chouhan A S, Jasti N P and Avasthi S 2018 Effect of interface defect density on performance of perovskite solar cell: Correlation of simulation and experiment. *Mater. Lett.* 221: 150–153

[22] Paquin F, Rivnay J, Salleo A, Stingelin N and Silva C 2015 Multi-phase semicrystalline microstructures drive exciton dissociation in neat plastic semiconductors. *J. Mater. Chem. C* 3: 10715–10722

[23] Qiu Z, Xu Z, Li N, Zhou N, Chen Y, Wan X, Liu J, Hao X, Bi P, Chen Q, Cao B and Zhou H 2018 Monolithic perovskite/Si tandem solar cells exceeding 22% efficiency via optimizing top cell absorber. *Nano Energy* 53: 798–807

[24] Bett A J, Schulze P S C, Winkler K M, Kabakli W O, Ketterer I, Mundt L E, Reichmuth K, Siefer G, Cojocaru L, Tutsch L, Bivour M, Hermle M, Glunz S W and Gold-schmidt J C 2020 Two-terminal Perovskite silicon tandem solar cells with a high-Bandgap Perovskite absorber enabling voltages over 1.8 V. *Prog. Photovoltaics Res. Appl.* 28(2): 99–110

[25] Shrivastav N, Madan J, Pandey R and Shalan A E 2021 Investigations aimed at producing 33% efficient perovskite-silicon tandem solar cells through device simulations. *RSC Adv.* 11(59): 37366–37374

[26] Burgelman M, Nollet P and Degrave S 2000 Modelling polycrystalline semiconductor solar cells. *Thin Solid Films* 361: 527–532

[27] Mouchou R T, Jen T C, Laseinde O T and Ukoba K O 2021 Numerical simulation and optimization of p-NiO/n-TiO₂ solar cell system using SCAPS. *Mater. Today Proc.* 38: 835–841

[28] Mazumder S and Senthilkumar K 2022 Device study and optimisation of CZTS/ZnS based solar cell with CuI hole transport layer for different conduction band offset. *Sol. Energy* 237: 414–431

[29] Lee S W, Bae S, Hwang J K, Lee W, Lee S, Hyun J Y, Cho K, Kim S, Heinz F D, Choi S B, Choi D, Yang J, Jeong S, Park S J, Schubert M C, Glunz S, Kim W M, Kang Y and Lee H S 2020 Perovskites fabricated on textured silicon surfaces for tandem solar cells. *Commun. Chem.* 3(1): 1–11

[30] Husainat A, Ali W, Cofie P, Attia J and Fuller J 2019 Simulation and Analysis of Methylammonium Lead Iodide (CH₃NH₃PbI₃) Perovskite Solar Cell with Au Contact Using SCAPS 1D Simulator. *Am. J. Opt. Photonics* 7(2): 33

[31] Olyaeefar B, Ahmadi-Kandjani S and Asgari A 2017 Bulk and interface recombination in planar lead halide perovskite solar cells: A Drift-Diffusion study. *Phys. E Low-Dimensional Syst. Nanostructures* 94: 118–122

[32] Siekmann J, Ravishankar S and Kirchartz T 2021 Apparent Defect Densities in Halide Perovskite Thin Films and Single Crystals. *ACS Energy Lett.* 6(9): 3244–3325

[33] Madan J, Singh K and Pandey R 2021 Comprehensive device simulation of 23.36% efficient two-terminal perovskite-PbS CQD tandem solar cell for low-cost applications. *Sci. Rep.* 11(1): 1–13

[34] Meyer E, Mutukwa D, Zingwe N and Taziwa R 2018 Lead-free halide double perovskites: A review of the structural, optical, and stability properties as well as their viability to replace lead halide perovskites. *Metals (Basel)* **8**(9)

[35] Chaudhary N, Chaudhary R, Kesari J P, Aa Patra and Chand S 2015 Copper thiocyanate (CuSCN): an efficient solution-processable hole transporting layer in organic solar cells. *J. Mater. Chem. C* 3(45): 11886–11892

[36] Köhler M, Pomaska M, Procel P, Santhergen R, Zamchiy A, Lambertz A, Duan W, Cao P, Klingebiel B, Li S, Eberst A, Luysberg M, Qiu K, Isabella O, Finger F, Kirchartz T, Rau U and Ding K 2021 A silicon carbide-based highly transparent passivating contact for crystalline silicon solar cells approaching efficiencies of 24%. *Nat. Energy* 6(5): 529–537

[37] Furube A, Yoshinaga T, Kanehara M, Eguchi M and Teranishi T 2012 Electric-field enhancement inducing near-infrared two-photon absorption in an indium-tin oxide nanoparticle film. *Angew. Chemie - Int. Ed.* 51(11): 2640–2642

[38] Pandey R, Singla A, Madan J, Sharma R and Chaujar R 2019, Toward the design of monolithic 23.1% efficient hysteresis and moisture free perovskite/c-Si HJ tandem solar cell: A numerical simulation study. *J. Micromechanics Microengineering* **29**(6B)

[39] Korte L, Albrecht S, Crossland E, Stannowski B, Snaith H J and Case C 2019 Infrared Light Management Using a Nanocrystalline Silicon Oxide Interlayer in Monolithic

Perovskite/Silicon Heterojunction Tandem Solar Cells with Efficiency above 25%. *Adv. Energy Mater.* 9(14): 1–9

[40] Madhavan V E, Zimmermann I, Baloch A A B, Manekkathodi A, Beaidi A, Tabet N and Nazeeruddin M K 2020 CuSCN as Hole Transport Material with 3D/2D

Perovskite Solar Cells. *ACS Appl. Energy Mater.* 3(10): 114–121

[41] Burdick J and Glatfelter T 1986 Spectral response and I-V measurements of tandem amorphous-silicon alloy solar cells. *Sol. Cells* 18(3–4): 301–314